



Electrochemical micromachining of titanium microstructures in an NaCl–ethylene glycol electrolyte

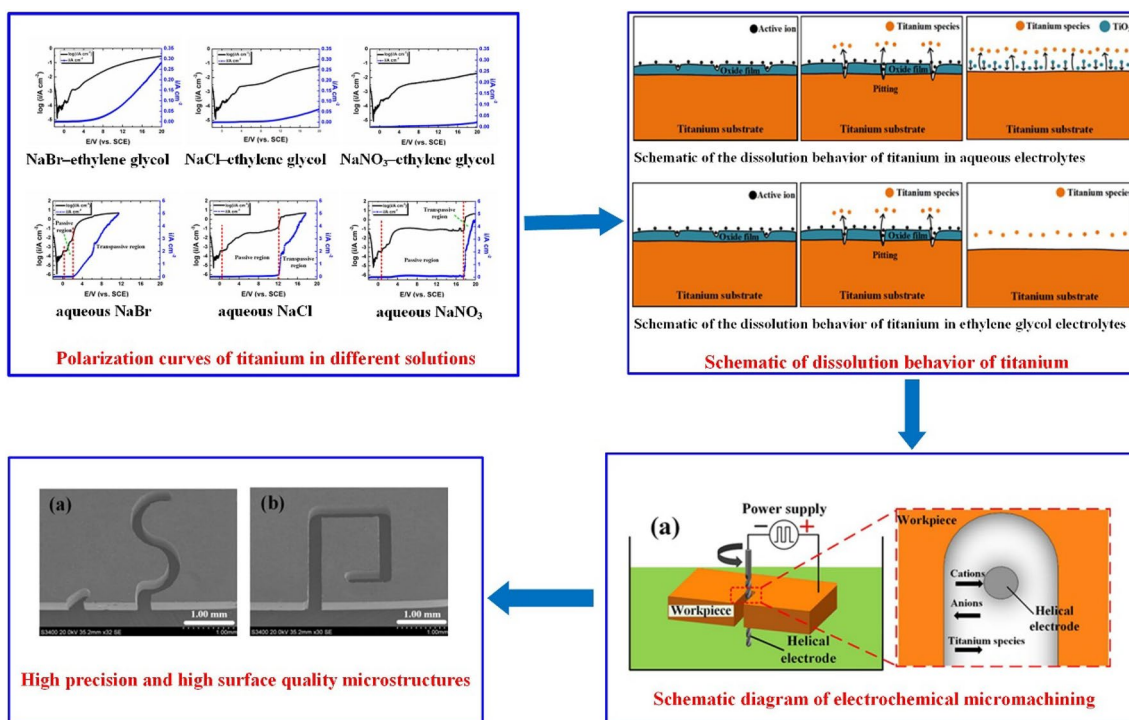
Ning Yu¹ · Xiaolong Fang^{1,2} · Lingchao Meng¹ · Yongbin Zeng^{1,2} · Di Zhu^{1,2}

Received: 19 September 2017 / Accepted: 4 January 2018 / Published online: 18 January 2018
© Springer Science+Business Media B.V., part of Springer Nature 2018

Abstract

Titanium and its alloys are widely used in the aerospace and biomedical industries owing to their outstanding corrosion resistance and good biocompatibility. Wire electrochemical micromachining (Wire-ECMM) is a promising method for fabricating titanium microstructures because of the absence of residual stress and tool wear. The electrochemical dissolution characteristics and polarization curves of titanium in aqueous and ethylene glycol-based electrolytes are obtained and analyzed. The effects of electrolyte anion species on electrochemical machining of pure titanium are experimentally evaluated. An NaCl–ethylene glycol electrolyte is selected to explore the influences of various process parameters on machining accuracy in ECMM. A rotary helical electrode is utilized to accelerate the removal of electrolysis products and thereby improve the refreshment of the electrolyte. Finally, titanium microstructures of high surface quality are fabricated with high precision using ECMM at a voltage of 11 V, a spindle rotation speed of 4000 rpm, a pulse frequency of 200 kHz, a duty ratio of 30%, and an electrode feed rate of 0.3 $\mu\text{m/s}$.

Graphical Abstract



Keywords Titanium · Wire electrochemical micromachining · Aqueous electrolyte · NaCl–ethylene glycol-based electrolyte · Microstructures

1 Introduction

Owing to high specific strength, excellent corrosion resistance, good fracture toughness, and light weight, titanium and its alloys have been used in the manufacture of engines blades [1, 2] and surface textures [3, 4]. However, as a result of their low thermal conductivity and high chemical reactivity with cutting tool materials, titanium and its alloys are difficult to machine [5]. The development of methods for the successful fabrication of titanium microstructures is thus a topic of great research interest [6].

Mechanical methods can encounter problems such as high tool wear, residual stress, among others [7]. In EDM and LBM, material is removed from the workpiece through melting and evaporation; as a result, there will be heat-affected zone and recast layers [8, 9].

Electrochemical micromachining (ECMM) is a non-traditional machining method in which the workpieces are shaped by controlled anodic dissolution [10]. It is independent of material strength and melting point, and produces structures without residual stress, tool wear, and heat-affected zone [11, 12]. These advantages make ECMM a promising approach for the fabrication of titanium microstructures. Various ECMM methods have been developed. In through-mask electrochemical machining (TMECM), material is dissolved away from uninsulated regions of a mask-patterned workpiece that forms the anode of an electrolytic cell. Madore and Landolt [13] and Madore et al. [14] adopted a TMECM process for fabricating microstructures consisting of cavities of diameter 30 μm and spiral-shaped channels of widths 30 μm on a titanium workpiece in a 3 M methanol–sulfuric acid electrolyte. Chen et al. [15] employed a through-mask electrochemical micromachining (TMEMM) approach with a 100 g/L NaNO_3 electrolyte, machining micro-dimples of diameter of 110 μm and depth 20 μm with optimized process parameters. Lu and Leng [16] utilized jet-electrochemical micromachining (Jet-ECMM) with an applied voltage of 200 V to produce deep micro-holes in titanium specimens. These methods have mainly been used to fabricate surface textures. Wire electrochemical machining, in which a metallic wire is used as the tool, can fabricate complex perforated structures under computer numerical control (CNC). Qu et al. [17] applied an axial electrolyte flushing method to machine titanium in a 2.5 wt% NaCl and 2.5 wt% NaNO_3 solution. However, this method has the disadvantages of a wide machining gap, the generation of pitting, and poor localization. Further study is needed to fabricate titanium microstructures.

Owing to the chemical reactivity of titanium, the anodic dissolution of titanium in different solutes and solvents has obtained more and more attention. Anasane and Bhattacharyya [6] investigated the nature of titanium dissolution in seven different solutes and solvents, and demonstrated that NaBr–ethylene glycol and NaBr + NaCl–ethylene glycol electrolytes are suitable for machining pure titanium through the experiments. Piotrowski et al. [18] studied the effect of some factors on the dissolution of titanium in a mixed electrolyte of sulfuric acid and methanol, including temperature, water concentration, H_2SO_4 , and Ti^{4+} concentration. Huang et al. [19] studied the dissolution characteristics of pure titanium in sulfuric acid–ethanol electrolytes and experiments showed that these are more stable and safer than sulfuric acid–methanol electrolytes. Fushimi and Habazaki [20] investigated the anodic dissolution of titanium in NaCl-containing ethylene glycol solution according to the polarization curves and found that the dissolution rate was determined by diffusion of titanium species.

However, there have been few systematic studies of the effect of solvent and anion type on the dissolution of pure titanium or on its ECM.

A serious problem that arises in ECMM concerns the removal of the products of electrolysis, which can affect the conductivity distribution. If these are not removed promptly, material dissolution will become uneven and machining accuracy will deteriorate. Even more seriously, there may be a complete failure of the machining process. There has been extensive research on methods to improve electrolyte refreshment, involving techniques such as axial electrolyte flushing [17], reciprocating traveling wires [21], tool vibration [22], cutting edge tools [23], and rotary helical electrodes [24, 25]. In particular, helical electrodes have proved to significantly accelerate the removal of electrolysis products. The rotation of helical electrode will result in electrolyte for circular and vertical movement, which can help to push the electrolysis products out along the spiral trajectory.

In this study, a rotary helical electrode is utilized to accelerate electrolyte refreshment. Electrolytes based on different solvents (ethylene glycol and water) and anions (bromide, chloride, and nitrate) are used, and the polarization curves of titanium in six different electrolytes are analyzed. Experiments are conducted to determine the most appropriate electrolyte and to investigate the effects of the process parameters on the width of machined slits. Finally, high-precision titanium microstructures are machined using the optimal parameters.

2 Electrochemical properties of titanium in different electrolytes

2.1 Principle of Wire-ECMM with a helical wire tool

A schematic diagram of Wire-ECMM with a helical wire tool is shown in Fig. 1a. The micro-graph of helical electrode is shown in Fig. 1b. The workpiece acts as the anode and the helical electrode as the cathode. During Wire-ECMM with a helical wire tool, the anodic workpiece is continuously dissolved and hydrogen bubbles are continuously generated on the surface of the helical electrode. The conductivity of the electrolyte is affected by these hydrogen bubbles and by the electrolysis products present in the machining gap. As the helical electrode rotates, the spiral grooves on its surface push the hydrogen bubbles, electrolysis products, and Joule heat generated in the machining gap out of the slot on the top of the workpiece, while fresh electrolyte is pulled in. The rotating helical electrode thus accelerates electrolyte refreshment and removal of electrolysis products, thereby making the electrical conductivity of the electrolyte in the machining gap more uniform, as well as improving process stability and machining accuracy [24, 25].

2.2 Polarization curves of titanium in different electrolytes

The composition and content of titanium was listed in Table 1 and titanium plates of thickness 0.5 mm were ultrasonically rinsed with acetone before the experiments. In order to investigate the dissolution characteristics of titanium in six electrolytes, anodic polarization curves

of titanium were obtained using a ZAHNER ZENNIUM electrochemical workstation. A platinum net and a calomel electrode were used as the counter electrode and reference electrode, respectively. All the tests were performed potentiodynamic with a scan rate of 50 mV/s, starting from -2 to 20 V. The polarization curves in the different electrolytes were shown in Fig. 2.

From the polarization curves, the following conclusions can be drawn:

- (1) In aqueous-based electrolytes, when the potential is close to 0, the workpiece has been entered passive region. The current density is close to 0 and barely increases with the increase of potential. But when passive film is destroyed, the workpiece enters transpassive region and the current density increases sharply with the increase of potential. In ethylene glycol-based electrolytes, due to the lack of water, passive film will not generate on the surface of workpiece. When the potential is less than the dissolution potential of titanium, the workpiece barely dissolves and the current density is close to 0. When the potential exceeds the dissolution potential, the workpiece is continuously dissolved and the current density increases with the increasing of potential.
- (2) The current density in aqueous electrolytes is much greater than in ethylene glycol electrolytes: of the order of A/cm^2 compared with mA/cm^2 .
- (3) The transpassivation potentials are in the order $NO_3^- > Cl^- > Br^-$. The different anions thus exhibit different abilities to disrupt the passive film, with bromide ion being the most powerful in this regard [13].

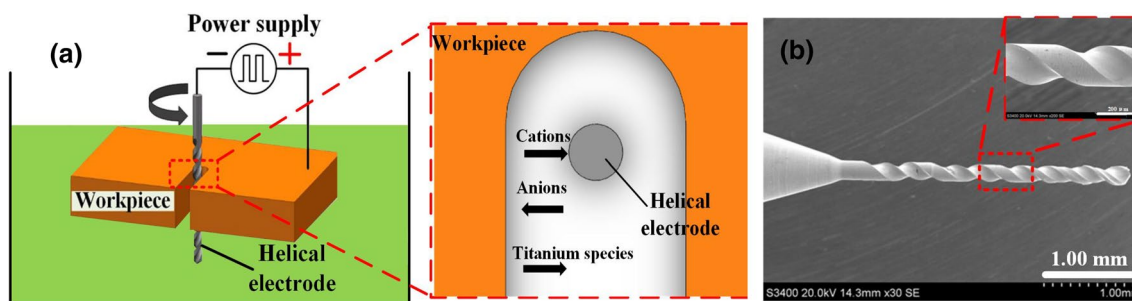


Fig. 1 Schematic diagram of Wire-ECMM with a helical wire tool and the micro-graph of helical electrode

Table 1 Composition and content of titanium

Composition	Ti	Fe	C	N	H	O	Other elements
Content	98.885%	0.3%	0.1%	0.05%	0.015%	0.25%	0.4%

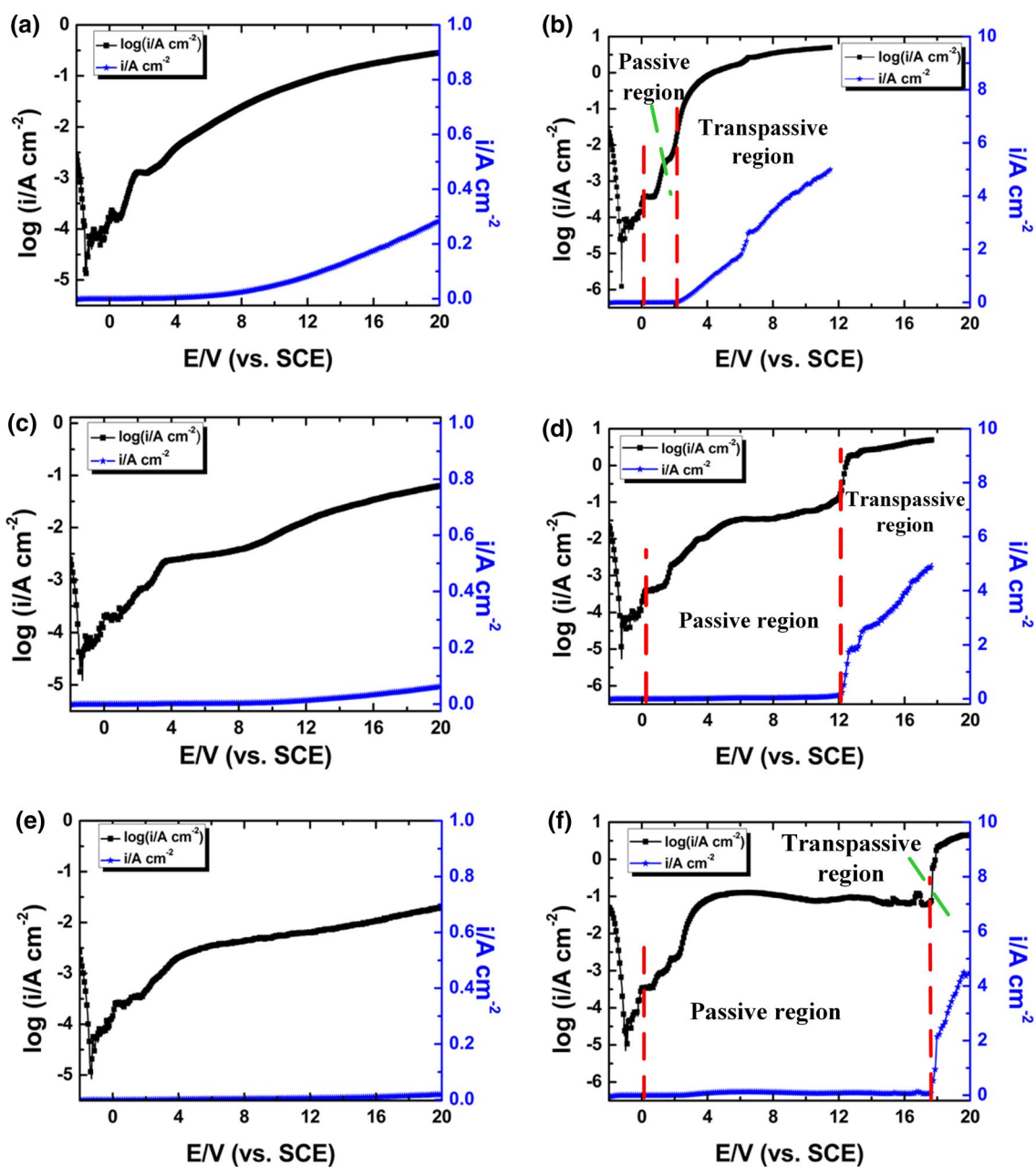


Fig. 2 Polarization curves in different electrolytes: **a** 1 mol/L NaBr–ethylene glycol; **b** 1 mol/L aqueous NaBr; **c** 1 mol/L NaCl–ethylene glycol; **d** 1 mol/L aqueous NaCl; **e** 1 mol/L NaNO₃–ethylene glycol; **f** 1 mol/L aqueous NaNO₃

2.3 Anodic dissolution of titanium in different electrolytes

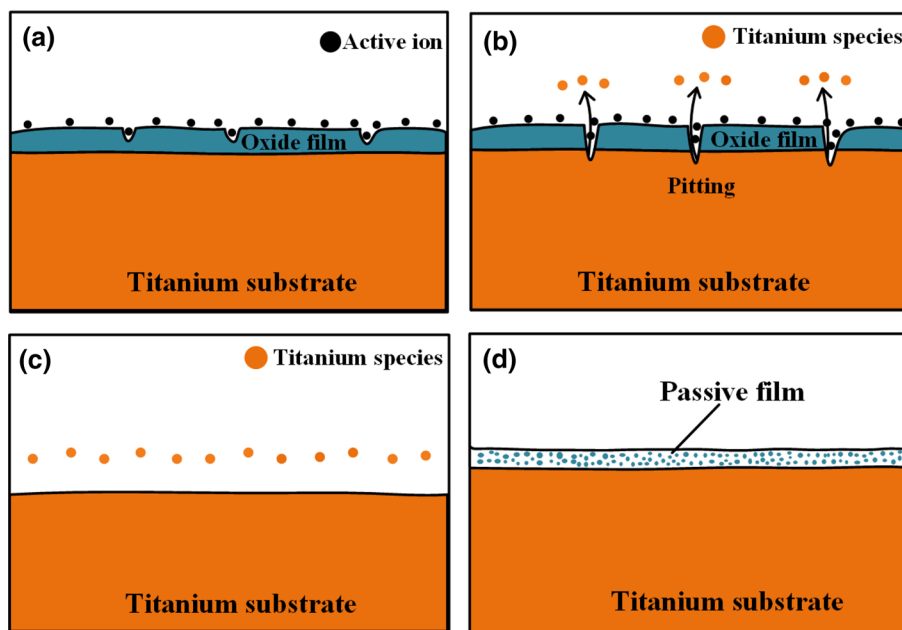
2.3.1 Anodic dissolution of titanium in aqueous solutions

When titanium is exposed to oxygen or an oxygen-containing environment, a dense oxide film is produced on its surface, with the result that titanium shows excellent corrosion resistance. However, the presence of this passive

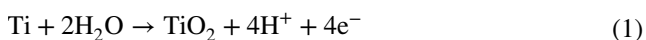
film also makes machining of titanium by anodic dissolution difficult [6]. A further problem results from adhesion of electrolysis products to the surface of the workpiece, and in ECM on a macroscopic scale, a high-speed flow of electrolyte is usually applied to wash away these products.

Figure 3 illustrates schematically the dissolution behavior of titanium in an aqueous electrolyte. At the beginning of ECM, active ions attach to defects on the oxide film, as shown in Fig. 3a. When the applied

Fig. 3 Schematic of the dissolution behavior of titanium in an aqueous electrolyte



machining potential is lower than the transpassivation potential, dissolution of titanium will be prevented by the passive oxide film. The thickness of this film grows linearly with the potential, until the transpassivation potential is reached, when pitting starts to appear at locations of higher current density, as shown in Fig. 3b. Breakdown of the film then takes place and the titanium starts to dissolve [26], as shown in Fig. 3c. As soon as the smooth anode surface has been exposed, a passive film starts to form again [20], as shown in Fig. 3d. There is general agreement that the passive film on the surface of titanium consists of TiO_2 [27], formed by the following reaction [18]:



Then, the dissolution of titanium workpiece and the generation of passive film take place alternately in electrochemical machining, as shown in Fig. 3c, d. Throughout the anodic dissolution process, the externally applied

electric field will accelerate the development of the oxide layer from titanium and hydroxide ions [6].

After ECM has been completed, an oxide film will be regenerated on the titanium surface.

2.3.2 Anodic dissolution of titanium in ethylene glycol solutions

The use of ethylene glycol instead of water can, on the one hand, help to avoid the generation of oxygen on the anode at low current densities, and, on the other hand, prevent contact between oxygen and titanium. Figure 4 illustrates schematically the dissolution behavior of titanium in an ethylene glycol electrolyte. As water is a source of passivating oxygen, ethylene glycol solutions are much less effective passivator. Hence, passive film is rarely generated after the smooth anode surface has been exposed, and titanium continues to dissolve, the machinability of titanium is better. The schematic of the dissolution behavior is shown in Fig. 4c.

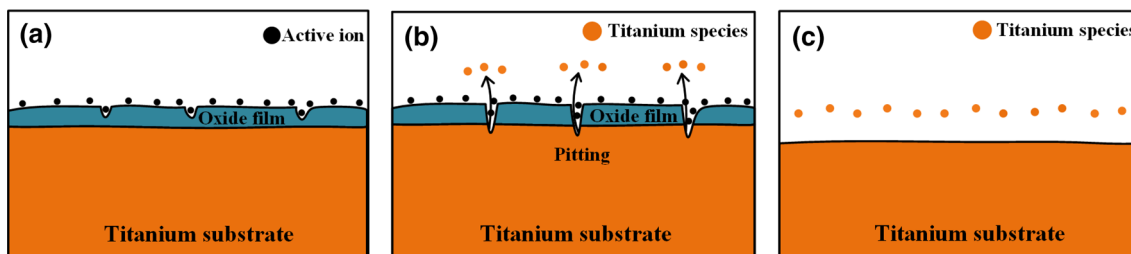


Fig. 4 Schematic of the dissolution behavior of titanium in an ethylene glycol electrolyte

2.4 Anodic dissolution of titanium with different anions

During Wire-ECMM with a helical wire tool, the cations move toward helical electrode, the anions move toward the workpiece, and the reaction product enters the electrolyte from the workpiece. The schematic diagram of electrochemical micromachining of titanium is shown in Fig. 1a.

The role of anions is reflected not only in the destruction of the passive film, but also in the subsequent dissolution of the titanium substrate. In aqueous electrolytes containing NaBr or NaCl, the anions can react with titanium and water to form titanium oxochloride compounds.

In ethylene glycol electrolytes containing NaBr or NaCl, products formed in electrochemical machining can react with ethylene glycol to yield soluble titanium glycolate [28].

3 Experimental setup and procedures

A schematic diagram of the Wire-ECMM with a helical wire tool experimental system is shown in Fig. 5a, a photograph of experimental apparatus is shown in Fig. 5b. Its principal components are an X–Y–Z movement stage, an air-bearing spindle, a pulsed power generator, an oscilloscope, a desktop computer, and a charge-coupled device (CCD) vision system. During machining, the helical electrode rotates with the air-bearing spindle, and the anodic titanium workpiece is fed through X–Y linear motion. The pulsed power generator supplies the electric voltage between the anode and cathode. The oscilloscope shows the applied voltage and the machining current waveform during the machining process. The machining condition is observed through the CCD vision system.

In this paper, the helical electrode used for the experiments was a commercial PCB micro drill (UNION TOOL, JAPAN). The diameter of the helical electrode was 200 μm .

During Wire-ECMM with a helical wire tool, if an electric short circuit occurred, the tool electrode was retracted to a constant distance, after which machining was restarted. If a short circuit occurred three times, this was defined as a failure of machining. The machining slits were measured five times separately by a measuring microscope (STM7, Olympus, Japan). Machined structures were measured by a scanning electron microscope (S-3400N, Hitachi, Japan).

Figure 6 is a schematic diagram of the Wire-ECMM with a helical wire tool, showing the machining gap, which can be calculated from the following relation:

$$\Delta_s = (s - d)/2, \quad (2)$$

where s is the slit width; Δ_s is the machining gap, and d is the diameter of the helical electrode; Δ_b is the inter-electrode frontal gap.

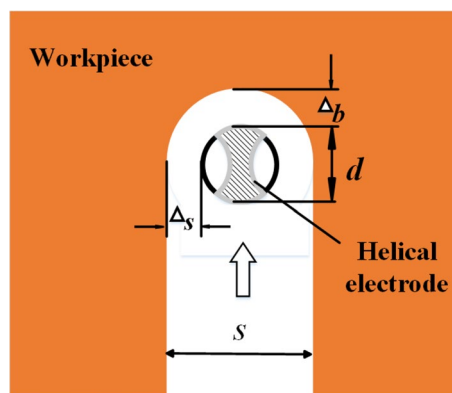


Fig. 6 Machining gap in Wire-ECMM with a helical wire tool

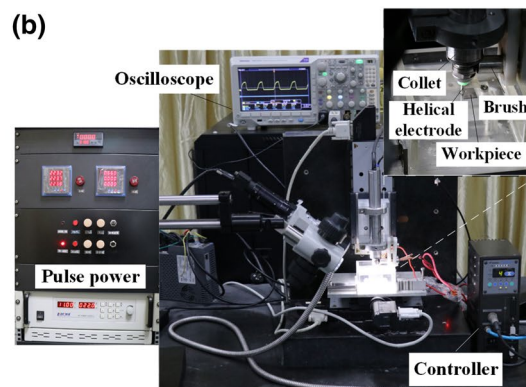
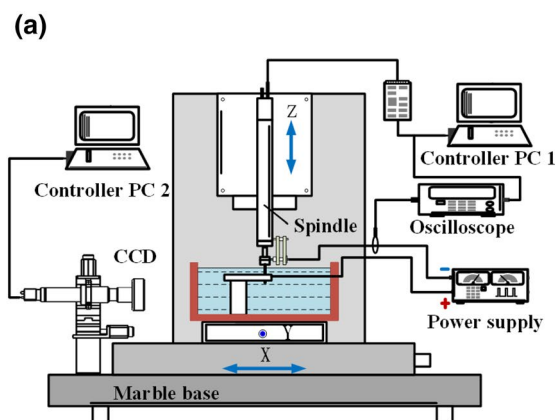


Fig. 5 Experimental apparatus for Wire-ECMM with a helical wire tool: **a** schematic diagram; **b** photograph

Table 2 Experimental machining parameters

Parameter	Value
Initial electrode gap	40 μm
Electrode diameter	0.2 mm
Applied voltage	20 V
Pulse frequency	200 kHz
Duty ratio	30%
Spindle rotation speed	4000 rpm
Feed rate	0.3 $\mu\text{m/s}$

Table 3 Experimental machining parameters

Parameters	Value
Electrolyte	1 mol/L NaCl–ethylene glycol
Rotation speed	4000 rpm
Applied voltage	10–16 V
Pulse frequency	1, 10, 20, 50, 100, 200 kHz
Duty ratio	25, 30, 35, 40, 45, 50%
Feed rate	0.1, 0.2, 0.3 $\mu\text{m/s}$

4 Results and discussion

4.1 Machining titanium with different electrolytes

The machining parameters in different electrolytes are chosen and listed in Table 2.

Attempts were made to machine titanium plates in the different electrolytes, as shown in Fig. 7. As can be seen from Fig. 7c, f, the machining was failed in 1 mol/L aqueous NaNO_3 electrolyte and NaNO_3 –ethylene glycol electrolyte.

In 1 mol/L aqueous NaBr electrolyte, most of the workpiece was corroded and lack of apparent manufacturing marks. While in 1 mol/L NaBr–ethylene glycol, apparent manufacturing marks existed but the whole surface existed stray corrosion and the surface of titanium workpiece becomes flocculent, as shown in Fig. 7a, d.

In 1 mol/L aqueous NaCl electrolyte, the machining was failed, as shown in Fig. 7b. While in 1 mol/L

NaCl–ethylene glycol electrolyte, the machining was successful, as shown in Fig. 7e.

Due to the failure of machining in aqueous NaCl, NaNO_3 –ethylene glycol, and aqueous NaNO_3 electrolytes, further attempts were made to machine titanium in these electrolytes with the application of a higher voltage and/or duty ratio, while keeping other parameters (spindle rotation speed, pulse frequency, and so on) the same as in Table 3. Machining succeeded in aqueous NaCl, with the results shown in Fig. 8, but failed in NaNO_3 –ethylene glycol and aqueous NaNO_3 .

The following conclusions can be drawn from these experimental results:

- (1) Titanium can be machined successfully in aqueous NaCl electrolyte at a higher voltage and duty ratio. However, serious stray corrosion occurred during ECMM, with poor uniformity of the slits, which were jagged, as shown in Fig. 8. Thus, a 1 mol/L aqueous NaCl electrolyte is unsuitable for machining titanium.

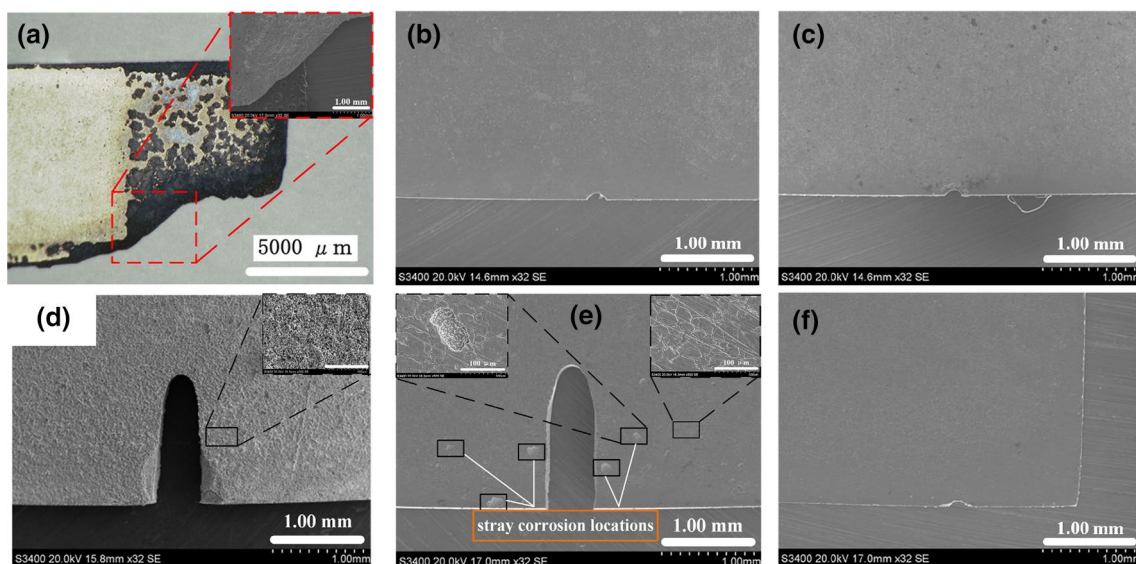
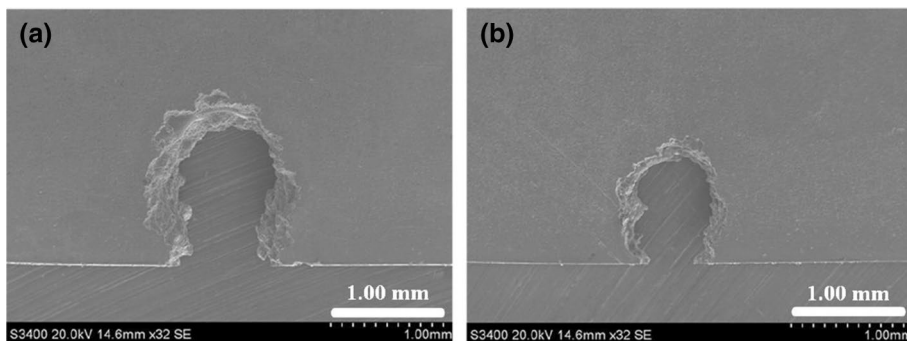


Fig. 7 Influence of different electrolytes on the machined slits: **a** 1 mol/L aqueous NaBr; **b** 1 mol/L aqueous NaCl; **c** 1 mol/L aqueous NaNO_3 ; **d** 1 mol/L NaBr–ethylene glycol; **e** 1 mol/L NaCl–ethylene glycol; **f** 1 mol/L NaNO_3 –ethylene glycol

Fig. 8 Slits machined in aqueous NaCl electrolyte at higher voltage and/or duty ratio: **a** 25 V, 30%; **b** 25 V, 40%



- (2) In 1 mol/L aqueous NaBr electrolyte, most of the workpiece was corroded and lack of apparent manufacturing marks, as shown in Fig. 7a. Because Br^- in solution helps disrupt the passive film and the current density have increased to 5 A/cm^2 when the potential only increased to about 11 V, as shown in Fig. 2b. Consequently, 1 mol/L aqueous NaBr solution is also unsuitable for machining titanium.
- (3) According to Fig. 7d, e, NaBr–ethylene glycol and NaCl–ethylene glycol electrolytes are suitable for machine titanium. However, in NaBr–ethylene glycol, the whole surface existed stray corrosion and the surface of workpiece becomes flocculent, whereas in NaCl–ethylene glycol, pitting only existed in five locations around the machining region. Furthermore, the uniformity of the slit machined in the NaBr–ethylene glycol electrolyte was poor compared with that machined in NaCl–ethylene glycol. In summary, the 1 mol/L NaCl–ethylene glycol electrolyte was the most suitable of those tested to machine titanium, and pitting can be eliminated by optimizing the experimental parameters in this electrolyte.

4.2 Parametric study of Wire-ECMM with a helical wire tool of pure titanium in NaCl–ethylene glycol electrolyte

According to the classical electrochemical machining theory,

$$\Delta_b = \eta \omega \kappa U / v \quad (3)$$

$$s \approx d + 2\Delta_b \sqrt{2d/\Delta_b + 1}, \quad (4)$$

where Δ_b is the inter-electrode frontal gap; v is the cathode feed rate in the balanced state; η is the current efficiency; ω is the electrochemical equivalence of the anode metal; κ is the electrolyte conductivity; U is the applied voltage; d is the diameter of tool electrode, and s is the slit width.

According to Eqs. (2–4), the machining gap is related to electrical parameters and feed rate. Hence, the effects of electrical parameters and feed rate on slits machined in a 1 mol/L NaCl–ethylene glycol electrolyte were investigated.

According to the previous helical electrode experiments study conducted by Fang et al. [26, 27] and the polarization characteristic in NaCl–ethylene glycol electrolyte in this work, these parameters and their values are chosen and listed in Table 3.

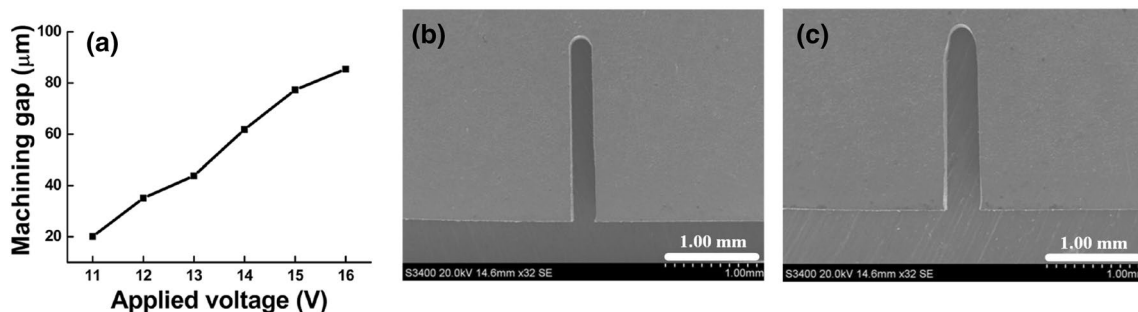


Fig. 9 Effect of applied voltage on machining gap: **a** the variation of machining gap versus applied voltage; **b** SEM of machined slit at applied voltage of 11 V; **c** SEM of machined slit at applied voltage of 16 V

4.2.1 Effect of applied voltage on machining gap

According to Eqs. (2–4), inter-electrode frontal gap (Δ_b) is proportional to applied voltage (U) and the slit width (s) is positively related to inter-electrode frontal gap (Δ_b). Hence, the slit width (s) is positively related to applied voltage (U) and the machining gap (Δ_s) is positively related to applied voltage (U). The machining gap increases with the increasing of applied voltage.

Figure 9a shows the machining gap at different applied voltages for a rotation speed of 4000 rpm, a pulse frequency of 200 kHz, a duty ratio of 30%, and a feed rate of 0.3 $\mu\text{m/s}$. At an applied voltage of 11 V, the inter-electrode gap was 20.1 μm , and a high surface quality could be achieved without pitting, as shown in Fig. 9b. At an applied voltage of 16 V, the inter-electrode gap increased to 85.4 μm , as shown in Fig. 9c. However, at an applied voltage of 10 V, electrical short circuits occurred frequently during the machining. In the rest of this paper, 11 V will be taken as the optimal voltage for machining titanium.

4.2.2 Effect of pulse frequency on machining gap

The pulse frequency, especially the nano-second pulse, has an important effect on the machining accuracy [29, 30]. Increase in frequency causes reduction in pulse period, which can increase the localization [31]. The relationship between pulse frequency and inter-electrode gap was studied at a fixed machining voltage of 11 V, spindle rotation speed of 4000 rpm, duty ratio of 30%, and feed rate of 0.3 $\mu\text{m/s}$. Fig. 10a shows the machining gap at different pulse frequencies. When the pulse frequency was 1 kHz, the inter-electrode gap was 93.1 μm and stray corrosion pits were formed, as shown in Fig. 10b. The minimum inter-electrode gap of 20.1 μm was obtained at a pulse frequency of 200 kHz, with high surface quality without pitting being achieved, as shown in Fig. 10c. Thus, 200 kHz was taken as the optimal pulse frequency.

4.2.3 Effect of duty ratio on machining gap

Due to the increase in duty ratio, on-time of pulse period increases that in turn increases the dissolution rate [31]. Figure 11a shows the machining gap at different duty ratios for a machining voltage of 11 V, a spindle rotation speed of 4000 rpm, a pulse frequency of 200 kHz, and a feed rate

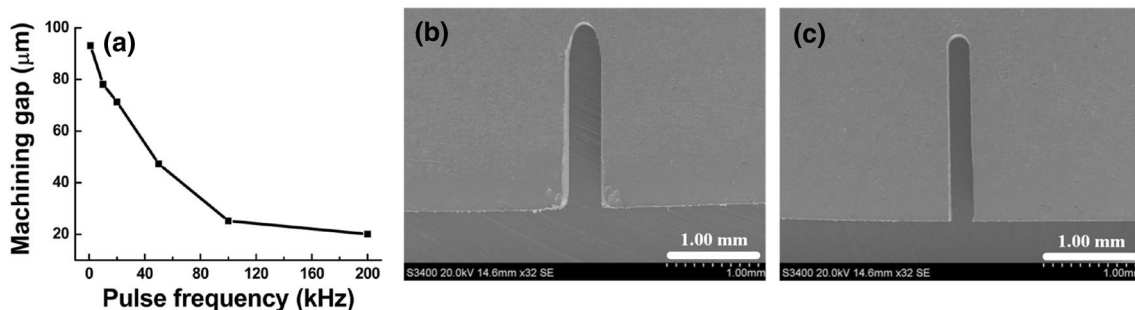


Fig. 10 Effect of pulse frequency on machining gap: **a** the variation of machining gap versus pulse frequency; **b** SEM of machined slit at pulse frequency of 1 kHz; **c** SEM of machined slit at pulse frequency of 200 kHz

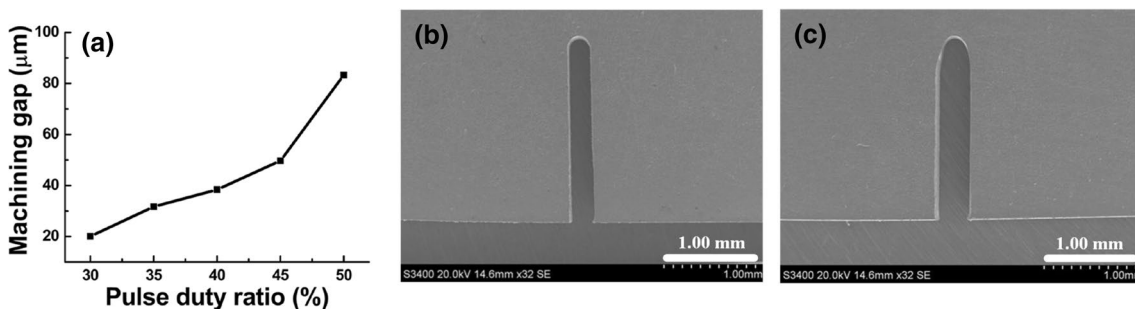


Fig. 11 Effect of duty ratio on machining gap: **a** the variation of machining gap versus pulse duty ratio; **b** SEM of machined slit at pulse duty ratio of 30%; **c** SEM of machined slit at pulse duty ratio of 50%

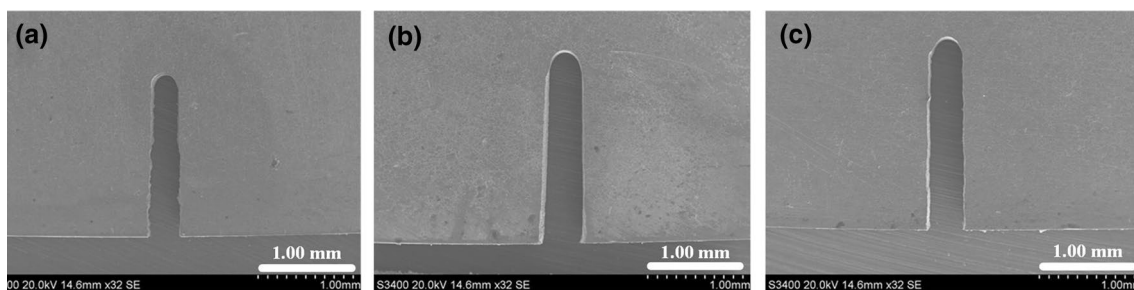
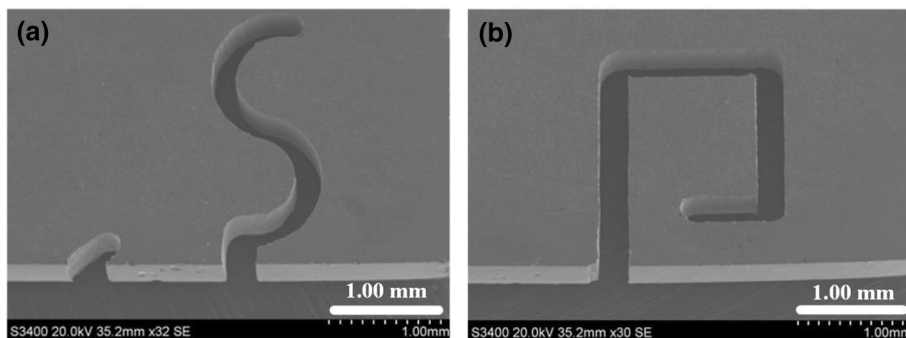


Fig. 12 The SEM pictures of machined slits with the feed rate of **a** 0.1 $\mu\text{m/s}$; **b** 0.2 $\mu\text{m/s}$; **c** 0.3 $\mu\text{m/s}$

Fig. 13 SEM pictures of the microstructures: **a** “S” shape; **b** square spiral



of 0.3 $\mu\text{m/s}$. The minimum inter-electrode gap of 20.1 μm was attained at a duty ratio of 30%, as shown in Fig. 11b. When the duty ratio increased to 50%, the inter-electrode gap increased to 83.3 μm , as shown in Fig. 11c. However, at a duty ratio of 25%, there was very little machining time per cycle, and there were frequent electrical short circuits during machining. Consequently, the optimal duty ratio was taken as 30%.

4.2.4 Effect of electrode feed rate on machining gap

For stable electrochemical machining, the rate of anodic material dissolution should be equal to the feed rate of the tool electrode. According to Eqs. (2–4), inter-electrode frontal gap (Δ_b) is inversely proportional to feed rate (v) and the slit width (s) is positively related to inter-electrode frontal gap (Δ_b). Hence, the slit width (s) is inversely positively related to feed rate (v) and the machining gap (Δ_s) is inversely positively related to feed rate (v). The machining gap decreases with the increasing of electrode feed rate.

The relationship between pulse frequency and inter-electrode gap was studied at a fixed machining voltage of 14 V, a spindle rotation speed of 4000 rpm, a pulse frequency of 200 kHz, and a duty ratio of 30%. Figure 12 shows the machining slits at different feed rates. When the feed rate was 0.1 and 0.2 $\mu\text{m/s}$, the uniformity of the slit was poor. When the feed rate was 0.3 $\mu\text{m/s}$, the uniformity of the slit was improved and the slit was narrow.

4.3 Fabrication of titanium microstructures

Finally, microstructures of high surface quality were fabricated with high precision in 1 mol/L NaCl–ethylene glycol electrolyte at a voltage of 11 V, a spindle rotation speed of 4000 rpm, a pulse frequency of 200 kHz, a duty ratio of 30%, and an electrode feed rate of 0.3 $\mu\text{m/s}$. The results are shown in Fig. 13.

5 Conclusions

This paper has investigated the use of a helical cathode in various electrolytes for the high-precision fabrication of microstructures in titanium. The following conclusions can be drawn from the results of this study:

- (1) The polarization curves in six different electrolytes have been obtained and analyzed.
- (2) The anodic dissolution characteristic in aqueous-based electrolytes and ethylene glycol-based electrolytes has been illustrated.
- (3) According to experiments in different electrolytes and the analysis of polarization curves, the NaCl–ethylene glycol electrolyte is selected as the suitable electrolyte to machine titanium.

- (4) In 1 mol/L NaCl–ethylene glycol electrolyte, microstructures with high surface quality were successfully fabricated with high precision.

Acknowledgements The work described in this paper was supported by the Joint Funds of the National Natural Science Foundation of China and Guangdong Province (Grant U1601201).

References

1. Tetsui T, Shindo K, Kobayashi S (2002) *Scripta Mater* 47:399–403
2. Janschek P (2015) *Mater Today Proc* 2:S92–S97
3. Li HS, Gao CP, Wang GQ, Qu NS, Zhu D (2016) *Sci Rep* 6:35013
4. Sjöström T, Su B (2011) *Mater Lett* 65(23):3489–3492
5. Umbrello D (2008) *J Mater Process Technol* 196:79–87
6. Anasane SS, Bhattacharyya B (2016) *Int J Adv Manuf Technol* 86:1–14
7. Pramanik A (2014) *Int J Adv Manuf Technol* 70:919–928
8. Rajurkar KP, Sundaram MM, Malshe AP (2013) *Proc CIRP* 6:13–26
9. Liang SY, Shih AJ (2016) Springer, New York, pp. 193–206
10. Lohrengel MM, Rataj KP, Munninghoff T (2016) *Electrochim Acta* 201:348–353
11. Hong H, Tsai HY (2013) *Advanced analysis of nontraditional machining*. Springer, New York
12. Klocke F, Zeis M, Harst S, Klink A, Veselovac D, Baumgärtner M (2013) *Proc CIRP* 8:265–270
13. Madore C, Landolt D (1997) *J Micromech Microeng* 7:270–275
14. Madore C, Piotrowski O, Landolt D (1999) *J Electrochem Soc* 146:2526–2532
15. Chen XL, Qu NS, Hou ZB (2017) *Int J Adv Manuf Technol* 88:565–574
16. Lu X, Leng Y (2005) *Mater Process Technol* 169:173–178
17. Qu NS, Ji HJ, Zeng YB (2013) *Chin J Aeronaut* 26:224–229
18. Piotrowski O, Madore C, Landolt D (1998) *J Electrochem Soc* 145:2362–2369
19. Huang CA, Hsu FY, Yu CH (2011) *Corros Sci* 53:589–596
20. Fushimi K, Habazaki H (2008) *Electrochim Acta* 53:3371–3376
21. Qu NS, Ji HJ, Zeng YB (2014) *Int J Adv Manuf Technol* 72:677–683
22. Natsu W, Nakayama H, Yu Z (2012) *Int J Precis Eng Manuf* 13:1131–1136
23. Zou XH, Fang XL, Zeng YB, Zhu D (2017) *Int J Adv Manuf Technol* 91:3943–3952
24. Fang XL, Zou XH, Zhang PF, Zeng YB, Qu NS (2016) *Int J Adv Manuf Technol* 84:929–939
25. Fang XL, Zhang PF, Zeng YB, Qu NS, Zhu D (2015) *J Mater Process Technol* 227:129–137
26. Kibra G, Bhattacharyya B, Davion JP (eds) (2017) *Non-Traditional Micromachining Processes*. Springer, Berlin, pp 337–365
27. Aladjem A (1973) *J Mater Sci* 8:688–704
28. Cotton FA, Wilkinson G (1999) *Advanced inorganic chemistry*, 6th edn. Wiley, New York
29. Hotoiu EL, Damme SV, Albu C, Deconinck D, Demeter A, Deconinck J (2013) *Electrochim Acta* 93:8–16
30. Hotoiu EL, Deconinck J (2014) *J Appl Electrochem* 44:1225–1238
31. Malapati M, Bhattacharyya B (2011) *Mater Manuf Process* 26(8):1019–1027

Affiliations

Ning Yu¹ · Xiaolong Fang^{1,2} · Lingchao Meng¹ · Yongbin Zeng^{1,2} · Di Zhu^{1,2}

✉ Xiaolong Fang
xlfang@nuaa.edu.cn

² Jiangsu Key Laboratory of Precision and Micro-Manufacturing Technology, Nanjing 210016, China

¹ College of Mechanical and Electrical Engineering, Nanjing University of Aeronautics and Astronautics, 29 Yudao St., P.O. Box 1005, Nanjing 210016, China